Effect of Torsional Oscillations and Aging Time on the Steady State creep Characteristics of Cu – 2 wt% Be – 0.3 wt% Co alloy

M. Sobhy[a], M. A. Mahmoud[a], A. F. Abd El-Rehim[a] and A.M.El-Refai[*b]

[a]Physics Department, Faculty of Education, Ain Shams University, Cairo, Egypt.
[b] Physics Department, Faculty of women for Art, Science and Education, Ain Shams University,
amnaelrefai@yahoo.com

In the present study, the effect of torsional oscillations of low frequencies on the creep behavior of pre-aged Cu–Be–Co alloy has been studied. After solution heat treatment at 1073 K for 2h, samples were rapidly quenched into iced water. The quenched samples were immediately aged at 593 K for various periods (t_a = ½, 1, 2, 6, 40 h). The influence of torsional oscillations of increasing frequencies (0.90–5.30 Hz) on the steady state creep behavior was systematically examined at different testing temperatures (363 to 453 K). The experimental results of the investigation demonstrate that the steady state strain rate, $\acute{\varepsilon}_{st}$, has been enhanced with increasing the frequency of torsional oscillations. The value of activation energy is consistent with that quoted for dislocation intersection mechanism.

1. Introduction

With the new requirements of society and science, it is an important task for scientists and engineers to develop more high-performance metallic materials [1]. In recent years, some researchers have focused on improving the strength of materials by plastic testing such as equal channel angular pressing [2,3] and dynamic plastic testing [4,5]. Among all data available, it can be seen that Cu-Be alloys have the widest ultimate tensile strength (UTS) range up to 1558 MPa [6]. Therefore, the wide UTS range of Cu–Be alloy makes it possible to optimize its strength by different heat treatment conditions. Recently, many high-strength Cu–Be alloys have been fabricated and some of them have applied successfully. One of these materials is the Beryllium-bronze alloy, which contains 1.25 – 2.25 wt% Be, up to 0.5 wt% Co and the balance being

Cu. The presence of such small amount of Co increases the toughness and/or plasticity of Cu-Be alloy which increasing its strength at same time, a matter that contradict to a trade-off between the strength and toughness [7]. Therefore, this alloy is particularly used for the manufacture of the tools where non-sparking properties are required and played an important role in engineering applications and is widely used for electrical connections, mechanical parts and injection molds for plastics on account of their combined strength and high electrical conductivity [8].

The precipitation of Cu – Be binary alloys occurs in both continuous and discontinuous modes. Continuous precipitation creates uniformly distributed fine particles in the copper matrix because of the following precipitation process: α (supersaturated) $\rightarrow$ GP zones (or γ''– precipitates) $\rightarrow$ meta stable γ'– phase $\rightarrow$ equilibrium γ– phase [9,10]. The sequence and morphology of precipitation depend mainly on aging temperature and aging time. The first phase to nucleate from a supersaturated Cu – Be solid solution is coherent Cu-rich GP zones [11]. Following the GP zones formation is the precipitation of the transition γ'– phase. Previous studies [12-14] showed that aging of Cu – Be system at 588 K is accompanying with the formation of GP zones which on further aging transformed into the intermediate plate-like γ'–precipitates. In addition, no direct transformation of GP zones to γ'– phase but GP zones dissolves into the α-phase firstly then γ'– phase begins to form [14]. The equilibrium γ– phase forms after the transition phases and its appearance indicates the over aging of the alloy [15]. It has been found that the transition γ'– phase transformed to the equilibrium γ– phase by means of lattice rearrangement followed by atomic ordering [16]. Shimizu et al [17] concluded that aging of Cu – 2 wt% Be alloy up to 603 K for 5 h is accompanying with the precipitation of the final equilibrium γ –phase. It is well known that [18,19] the presence of Co modifies the grain boundary structure, delayed the recrystillization temperature and retarded the continuous precipitation at aging temperature $\leq$ 623 K but does not affect mechanism of structural transformation.

It was found that Cu – Be alloys containing up to 1 wt% Be are not age hardenable, but from that point on up to 4 wt% Be workers reported increasing greater hardness increments on heat treatment [14-18]. Cu – Be – Co alloys containing about 2 wt% Be and 0.3 wt% Co exhibit an excellent hardening through aging after solutionizing [20]. The study of Bonfield and Edwards [21] showed that the hardness of Cu –1.81 wt% Be – 0.28 wt% Co alloy varies with aging time and goes through a maximum, after which a slow decrease in hardness was obtained with further increase in aging time. The maximum hardness found at aging temperature of 588 K at different aging times

depending on the test conditions. The effect of torsional oscillations of different low frequencies during creep tests has not been widely studied. In the present work, the most common heat-treatable copper alloy (Cu – 2 wt% Be – 0.3 wt% Co alloy) was chosen to make it in different strength levels and then study its mechanical properties under the effect of imposed torsional oscillations. The study is intended to provide some information about the steady state creep behavior of Cu – 2 wt% Be – 0.3 wt% Co alloy aged at different times with and without superimposed torsional oscillations of various low frequencies.

2. Experimental Procedure

The materials used were an electrolytic copper (99.99%), flaky beryllium and cobalt (99.99%). These materials were prepared in a high purity graphite crucible to have the composition of Cu – 2 wt% Be – 0.3 wt% Co, melted by a high frequency vacuum furnace and then cast into an iron mould in vacuum. The alloy ingot of 1 cm diameter was homogenized in an argon atmosphere for 2 h at 1073 K and then subjected to hot-forging, annealing (for 30 hr at 1073 K in vacuum), hot-rolling, annealing (the same as before) and cold-rolling. Finally, wires of $50x10^{-4}$ m diameter for creep tests and sheets of $300x10^{-6}$ m thick for transmission electron microscope (TEM) investigations were obtained. The samples (wires and sheets) were solution- treated for 2 h at 1073 K in vacuum followed by quenching into water at 273 K. The quenched samples were aged at 593 K for various periods (t_a = ½, 1, 2, 6, 40 h) in salt bath which is a mixture of nitrate and nitrite.

Thin foils for TEM were prepared from 3mm discs spark cut sample slices. The samples were then electrolytically polished using a TenuPol-3 (Struers) jet polishing machine operating at 25 volts, current of 0.1 A and at temperature of 273 K, using a polishing solution consisting of 5 ml phosphoric acid, 3 ml nitric acid and 2 ml acetic acid. TEM observations were carried out on a JEOL 100S operating at 100 kV.

Creep data were obtained using a convectional creep testing machine which was modified so that creep experiments without and with torsional oscillations of low frequencies could be carried out. The details of such a modified machine described elsewhere [22]. In such machine, a constant load corresponding to a stress of 507 MPa was applied to the lower end of the samples with test length of $50x10^{-3}$ m, while the upper end was subjected to an oscillatory motion using an electric motor supplied the crept samples oscillations of low frequencies ν = 0.00, 0.90, 1.90, 3.20 and 5.30 Hz. The shear strain amplitude φ affecting the tested sample calculated using the equation [23]:

$$\varphi = \frac{r A}{h d} \quad (1)$$

where *A* is the actual amplitude of the oscillating vane, measured by a travelling microscope, *r* being the radius of the wire, *d* its length and *h* is the half length of the vane [22]. Preliminary tests carried out to select shear strain amplitude φ within the elastic limit range [24]. The creep tests without and with torsional oscillations were carried out for each aging time at different testing temperatures T_t = 363, 393, 423 and 453 K to activate the creep process. The accuracy of temperature measurements was ±1 K.

3. Experimental Results

Creep tests for the Cu – 2 wt% Be – 0.3 wt% Co samples subjected to superimposed torsional oscillations of different frequencies ν = 0,0.9, 1.9, 3.2 and 5.3 Hz with a fixed shear strain amplitude ($\varphi = 5.83x10^{-4}$) within the elastic limit were performed until the steady state creep stage was attained. Representative creep curves obtained at testing temperature T_t = 363 K and aging temperature T_a = 593 K for samples aged at t_a = ½ and 40 h subjected to torsional oscillations of different frequencies at constant shear strain amplitude are shown in Fig.(1). The steady state strain rate ($\acute{\varepsilon}_{st}$) was determined from the slopes of the linear parts of the creep curves. The irregular shift of the values of steady state strain rate ($\acute{\varepsilon}_{st}$) with aging time (logarithmic scale) at different frequencies of the imposed torsional oscillations at different testing temperatures is shown in Fig. (2). This figure implies that:

- A monotonic shift toward higher strain was observed with increasing aging time except at t_a = 1h (ln t_a = 8.18) and 6 h (ln t_a = 9.98).
- The first higher values of $\acute{\varepsilon}_{st}$ observed at aging time t_a = ½ h (ln t_a = 7.49) followed with the first minimum of occurred at t_a = 1 h (ln t_a = 8.18).
- The second softening phenomenon determined at t_a = 2 h (ln t_a = 8.88), after which the second hardening phenomenon at 6h (ln t_a = 9.98) was located.
- At aging times greater than 6 h, a further increasing of $\acute{\varepsilon}_{st}$ values with t_a was detected.
- The hump attained at t_a = 2 h (ln t_a = 8.88) is usually higher compared with that obtained at t_a = ½ h (ln t_a = 7.49) whilst the drop occurred at t_a = 1 h is usually deeper than that at t_a = 6 h (ln t_a = 9.98).
- Taking into consideration the effect of testing temperature T_t the sequence curves is in general regular.
- For all tested samples, increasing of testing temperature T_t is accompanied with a proceeding softening process.
- Increasing the degrees of imposed oscillations increases the $\acute{\varepsilon}_{st}$ levels.

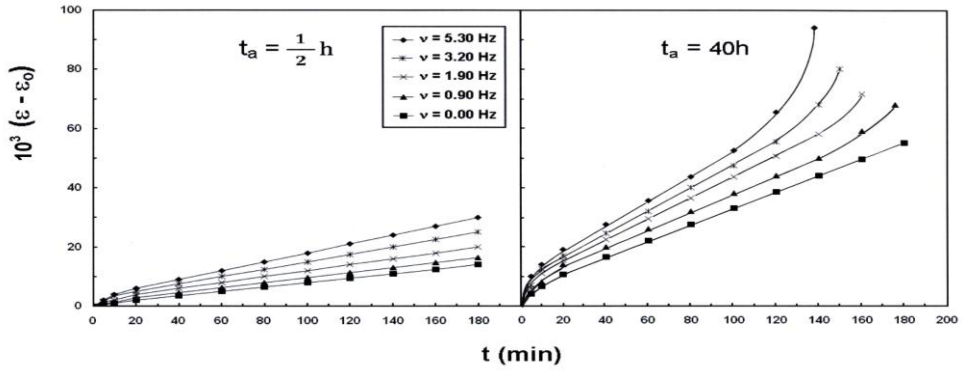

Fig. (1): Representative strain–time curves for Cu – 2 wt% Be – 0.3 wt% Co wire samles worked at testing temperature T_t = 363 K and aged at T_a = 593 K for aging time t_a = ½ and 40 h subjected to torsional oscillations of different frequencies (ν) at constant shear strain amplitude ($\varphi = 5.83x10^{-4}$).

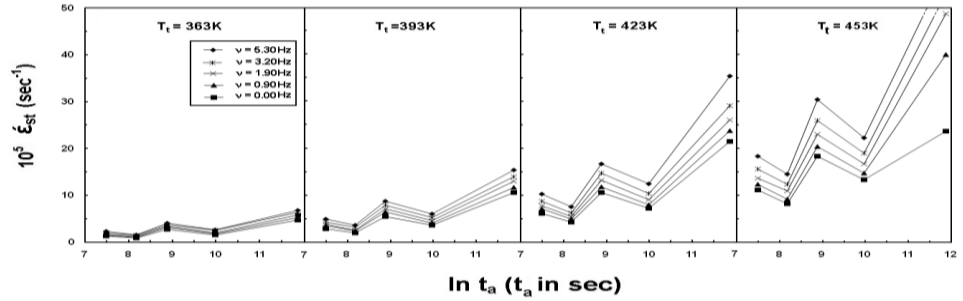

Fig. (2): Effect of aging time (ln t_a) on the steady state strain rate ($\dot{\varepsilon}_{st}$). Testing temperatures (T_t) and frequency of torsional oscillations (ν) are indicated.

The dependence of the steady state strain rate ($\dot{\varepsilon}_{st}$) values on the frequency of the imposed torsional oscillations (ν) at different aging times (t_a) is depicted in Fig.(3). It is evident from this figure that a gradual increment of $\dot{\varepsilon}_{st}$ values is observed with the increase in ν values. The influence of testing temperatures T_t (K) on the steady state creep rate ($\dot{\varepsilon}_{st}$) values at different aging times (t_a) is shown in Fig. (4). It is clear from Fig.4 that the sequence of curves for all aging times and frequencies applied is regular. In Figs (2–4), some $\dot{\varepsilon}_{st}$ values for t_a = 40 h are not included to allow clearance between the obtained results.

Figure (5) shows the precipitation of fine GP zones in sample aged at 593 K for ½ h. Fig. (6) shows the formation of coarsened GP zones in samples aged at 593 K for 1½ h, while Fig. (7) shows the presence of γ′–plates taken for samples aged at 593 K for 4 h. Fig. (8) shows γ –precipitates formed in samples aged at 593 K for 40 h.

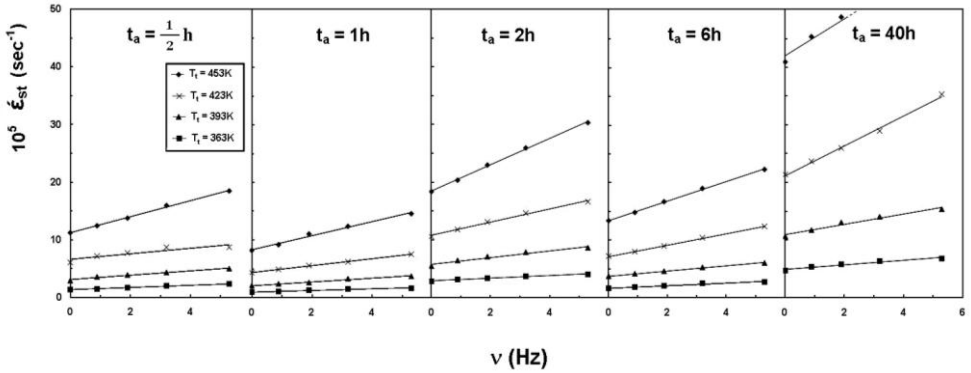

Fig. (3): Effect of frequency of torsional oscillations (ν) on the steady state strain rate ($\dot{\varepsilon}_{st}$). Aging times (t_a) and testing temperatures (T_t) are indicated.

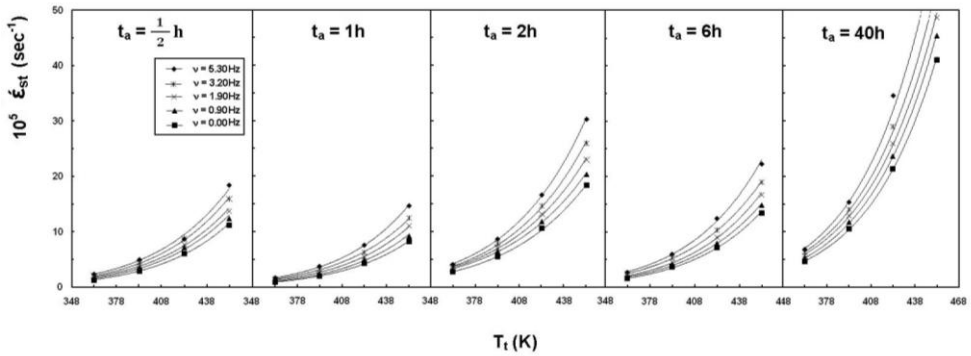

Fig. (4): Effect of testing temperature (T_t) on the steady state strain rate ($\dot{\varepsilon}_{st}$). Aging times (t_a) and frequencies of torsional oscillations (ν) are indicated.

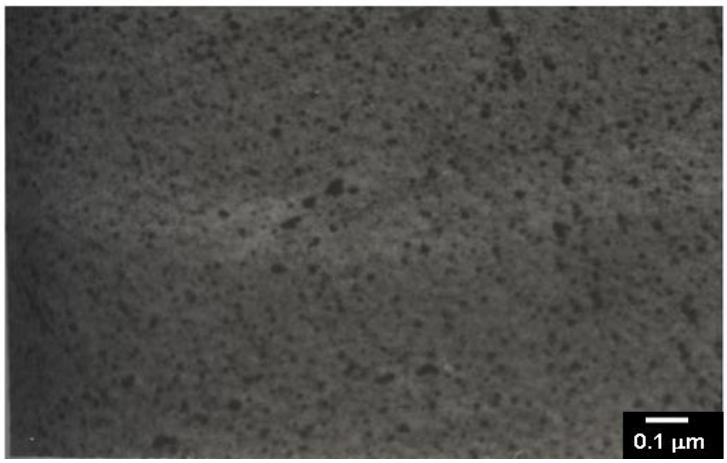

Fig. (5): TEM micrograph of Cu – 2 wt% Be – 0.3 wt% Co alloy aged at 593 K for ½ h showing the precipitation of fine G.P zones.

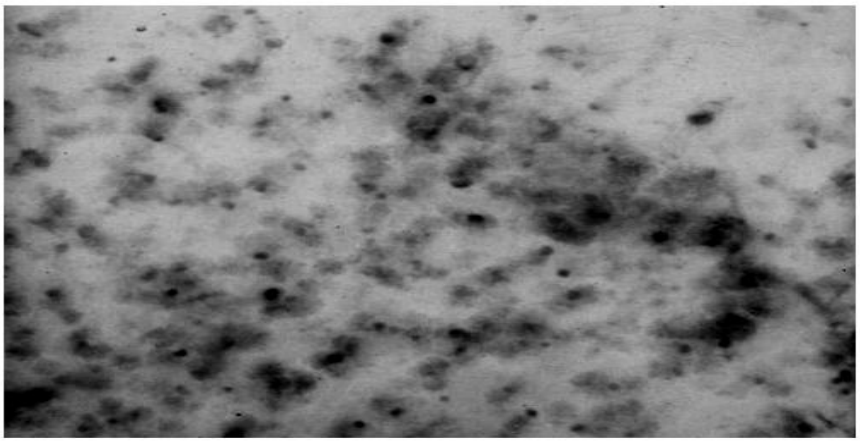

Fig. (6): TEM micrograph of Cu – 2 wt% Be – 0.3 wt% Co alloy aged at 593 K for 1½ h showing the precipitation of coarsened GP zones.

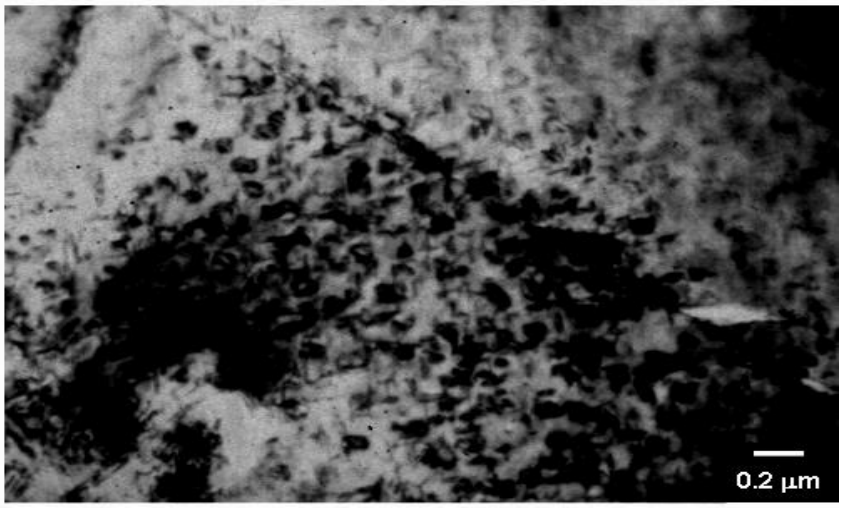

Fig. (7): TEM micrograph of Cu – 2 wt% Be – 0.3 wt% Co alloy aged at 593 K for 4 h showing the presence of γ′–plates.

4. Discussion

The behavior of the strain–time relations of Fig.(1) for Cu – 2 wt% Be – 0.3 wt% Co alloy is mainly controlled by the formation and/or growth of the existing phases [GP zones, γ′–phase and γ –phase] and their interactions with moving dislocations. These interactions play a great role in the resistance of the alloy to the recovery process. It is clear from Figs. (2) and 4 that the

serial irregularity of $\acute{\varepsilon}_{st}$ of alloy understudy is thermally activated as it depends on the pre-aging time and testing temperature. The curves presented in Fig.(2) emphasize that the structural changes take place during aging should have their own reflection on the steady state creep behavior. Thus, it is reasonable to correlate the values of steady state strain rate ($\acute{\varepsilon}_{st}$), with the variation of internal microstructure during aging process.

The sequence of structure transformation in supersaturated solid solution of Cu-Be alloy was found [26] to start with the formation of the spherical and equiaxed GP zones which are rich in solute atoms, coherent with matrix and differ from each other in thermal stability. For samples pre-aged at 593 K, the observed continuous decrease of $\acute{\varepsilon}_{st}$ with increasing pre-aging time from ½ to 1 h (first relaxation stage) for all worked testing temperatures could be attributed to the precipitation of fine dispersion equiaxed GP zones (see Fig. 5). The number, size, and distribution of these zones depend on the quenching rate and aging time. For t_a = ½ h and sever quench to 273 K, the number of GP zones – which act as pinners for moving dislocations– formed is relatively small and therefore the density of mobile dislocations is relatively large, as a result aging softening immediately takes place. With increasing aging time up to 1 h, the rate of hardening becomes very large as the number of fine zones increases gradually leading to a continuous decrease in the density of mobile dislocations [23].

In the second relaxation stage (1 h $\leq t_a \leq$ 2 h), the artificial aging of the quenched alloy gives rise to control the precipitation of the second phase with a high level of ductility. The increase in $\acute{\varepsilon}_{st}$ values in this aging time range can be explained as being due to the coarsening of GP zones on the expense of their number (see Fig.6) a matter that produces a matrix with small number of large grains. Accordingly, softening results since the dislocations slip planes become relatively clean from barriers allowing larger slip distances for dislocations [27].

In spite of the applied stress and torsional oscillations modify largely the effective forces in the material (as will be discussed), the tensile properties still depend mainly on the kind of second phase being coherent or incoherent with the matrix. Such types differ in the mode of interaction with glide dislocations existing in the matrix [28]. By further heating (2 h $< t_a \leq$ 6 h), the third relaxation stage starting with the observed decrease in the values of $\acute{\varepsilon}_{st}$ might be marked by the dissolution of GP zones and formation of small sized coherent γ'– precipitates (see Fig.7). Since the cutting of dislocations through the finer plate-like intermediate γ'– precipitates will be difficult, the hardening effects is observed as a decrease in the $\acute{\varepsilon}_{st}$ values [29].

The increase of steady state strain rate ($\acute{\varepsilon}_{st}$) with the shift to larger aging time ($6h < t_a \leq 40$ h) observed in Fig. (2) may be the result of the coarsening of the plate-like intermediate γ' –precipitates and the early precipitation of the equilibrium γ –phase as seen in Fig. (8). The softening behaviour within the fourth relaxation stage could be explained on the basis that at larger aging time, the density of mobile dislocation decreases since the size of precipitates become somewhat bigger resulting in a large decrease in the number of pinning points.

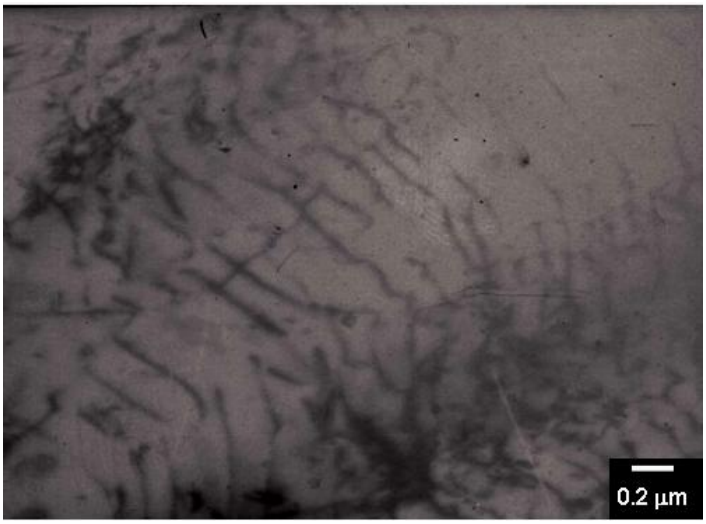

Fig. (8): TEM micrograph of Cu – 2 wt% Be – 0.3 wt% Co alloy aged at 593 K for 40 h showing the precipitation of γ –precipitates.

It is seen from Fig. (2) that under the same applied frequency and testing temperature, aging the samples at t_a = 2 h yields creep rate higher than those aged at t_a = ½ h. This behavior explains that GP zones decrease the average distances between dislocations by higher rates compared with coarser GP zones and small sized γ'– precipitates. Also, aging the samples at t_a = 1 h yields a harder matrix alloy than those aged at t_a = 6 h. These data established the fact that the matrix contains coarsened γ'– precipitates has high levels of dislocations density (i.e. high levels of $\acute{\varepsilon}_{st}$) compared with matrix contains coarsened GP zones.

The higher values of $\acute{\varepsilon}_{st}$ of the vibrating samples as compared to samples not subjected to torsional vibrations as in Fig. (3) may be due to: i) the fact that the additional elastic energy associated with the contentious vibration would be stored in the vibrating samples [29]. Such energy is expected to enhance the

process of re-arrangement of dislocations to form a more stable configuration of network through a redistribution of a small number of pinning agents (GP zones, γ′– and γ– precipitates) on the dislocation segment. This redistribution decreases the rate of interaction between the existing phases and moving dislocations and makes dislocation loop length will be in favor of amplifying the effective loops lengths, L_p. ii) The twisting motion of the imposed oscillations can allow additional interaction between the moving dislocation in the direction of stress and the other existing second phase particles in favor of large degree of softening. The twisting motion of dislocation segments can therefore make pining of dislocations less probable by the existing phases and vacancies dispersed in the matrix [30]. iii) The imposed oscillations are supposed to force the migration identities in a direction perpendicular to the direction of the axial stress which rearranges dislocation motion in the direction that increases $\acute{\varepsilon}_{st}$ [23].

At all testing temperatures worked and for all aging times used, increasing of $\acute{\varepsilon}_{st}$ with increasing the frequency of torsional oscillations as in Fig.3 may be explained as following: i) increasing the degree of torsional oscillations increases the rate of re-orientation of the already present dislocations in a more relaxed configuration very close to the tension axis. Therefore, the additional energy introduced by torsional testing maximize the mobility of the dislocations in the direction of the tension axis during creep process a matter that enhances the rate of recovery and shortens the duration of the process [31]. ii) By forcing the sample to vibrate with high frequency of torsional oscillations, the number of second phase particles per unit volume which act as obstacles for dislocation motion decrease by a relatively higher rate a matter that increases the average dislocation loop length, L_p by a higher rate. iii) Due to torsional testing, a large number of new dislocations is introduced to the matrix and move amongst the existing phases that are not able to block the movement of these dislocations very effectively through the pinning process [32]. These new dislocations continually generated by torsional testing having their maximum mobility in the direction that result in an increase $\acute{\varepsilon}_{st}$ levels.

It is clear from Fig. (4) that increasing of testing temperature lead to an increase of $\acute{\varepsilon}_{st}$ values providing an explanation that: i) the unpinning process is a thermally activated process where increasing the testing temperature increases the probability of dislocation to overcome the obstacles hindering its motion. So the dislocation moves longer distances during the action of work hardening and consequently the average slip distance loop is increased [33]. The increase in the volume of loop obtained reduces the average dislocation density and decreases the material resistance to flow [34]. ii) Increasing of testing

temperature helps annihilation of the already present dislocations by the formed ones induced by torsional oscillations and increases the rate of reorientation of the remaining dislocations in a more relaxed configuration far away from the tension axis [35]. iii) The increase of $\acute{\varepsilon}_{st}$ with increasing testing temperatures points towards the possibility that some ordering -due to thermal agitation of higher testing temperature- make haste motion of dislocations much easier [36].

As the creep curves obtained were significantly affected by different aging times used, hence the creep characteristics will depend mainly on the nature of the existing internal microstructure formed at these aging times. Consequently, for each aging time the testing temperature can be related to the energy activating the creep process in the steady state creep stage by the relation [25]:

$$\acute{\varepsilon}_{st} = \text{const. exp } (- E_{st}/RT_t) \qquad (2)$$

where R is the universal gas constant and T_t is the testing temperature in Kelvin. To estimate the average activation energy of steady state creep E_{st} for the present alloy, the slopes of straight lines relating ln $\acute{\varepsilon}_{st}$ and $1000/T_t$ given in Fig. (9) are evaluated. The slope of such straight lines give the energy activating creep process for samples crept at different frequencies of torsional oscillations. The calculated activation energies were found to be slightly different depending on either frequency of imposed oscillations or aging times and of average value ~ 34.5 kJ/mole. These nearly equal values of activation energy indicate that the structural changes take place during aging have no reflection on the mechanisms operating during the creep process. This value of activation energy is very close to the activation energy needed for dislocation intersection mechanism [37].

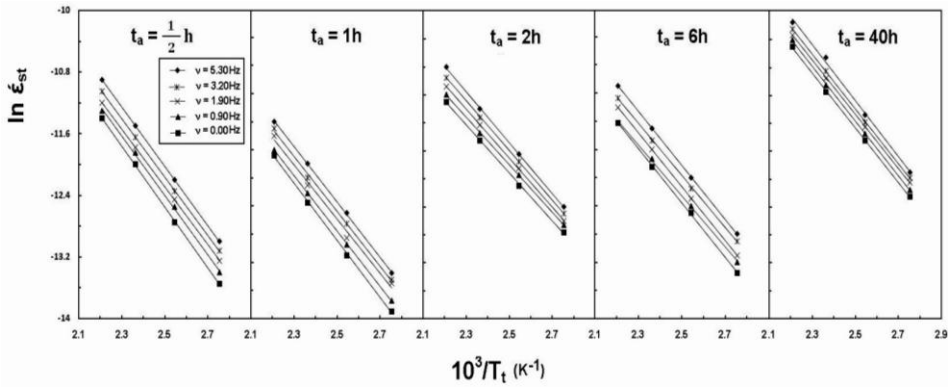

Fig. (9): A plot relates ln $\acute{\varepsilon}_{st}$ vs. $10^3/T_t$. Aging times (t_a) and frequencies of torsional oscillations (ν) are indicated.

5. Conclusions

The following conclusions have generally been made:

- The variation in the steady state strain rate, $\acute{\varepsilon}_{st}$, with increasing aging time was explained on the basis of structure transformations occuring in Cu–Be–Co alloy.
- For all test samples, increasing of testing temperature and/or frequency of imposed torsional oscillations is accompanied with a proceeding softening process.
- The obtained activation energy was ~ 34.5 kJ/mole characterizing dislocation intersection mechanism.

References

1. A. Kelly, R.B. Nicholson, Precipitation hardening, *Prog. Mater. Sci*., **10**, 3 (1963).
2. F. Dalla Torre, R. lapovok, J. Sandlin, P.F. Thomson, C.H.J. Davies, E.V. Pereloma, *Acta Mater*., **52**, 4819 (2004).
3. S. Qu, X.H. An, H.J. Yang, C.X. Huang, G. Yang, Q.S. Zang, Z.G. Wang, S.D. Wu, Z.F. Zhang, *Acta Mater*., **57**, 1586 (2009).
4. Y.S. Li, Y. Zhang, N.R. Tao, K. Lu, *Acta Mater*., **57**, 761 (2009).
5. G.H. Xiao, N.R. Tao, K. Lu, *Mater. Sci. Eng*. A **513**, 13 (2008).
6. J. C. Pang, Q. Q. Duan, S. D. Wu, S. X. Li, Z. F. Zhang, *Scripta Mat*., **63**, 1085 (2010).
7. B.Y. Huang, C.G. Shi, G.Z. Qiu, T.Y. Zuo, *China materials engineering canon Non-ferrous metal Engineering*, 4, (2005).
8. D. B. Williams, E. P. Butler, *Int. Met. Rev*., **26**, 153 (1981).
9. G. M. Li, S. J. Zinkle, *Comprehensive Nucl. Mater*., **4**, 667 (2012).
10. A. Varschavsky, E. Donoso, *Thermo. Acts*, **266**, 257 (1995).
11. R. J. Rioja, D. E. Laughlin, *Acta Metall*., **28**, 1301 (1980).
12. A. G. Khachaturyan, D. E. Laughlin, *Acta Metall. Mat*., **38**, 1823 (1990).
13. Y. M. Koo, J. B. Cohen, *Acta Metall*., 37 (1989) 1295.
14. S. Yamamoto, M. Matsui, Y. Murakami, *Trans. JIM*, **12**, 159 (1971).
15. Y. M. Koo, J. B. Cohen, S. M. Shapiro, *Acta Metall*., **36**, 591 (1988).
16. A. Yamamoto, H. Tusubakino, *Scr. Metall. Mater*. **31**, 787 (1994).
17. K. Shimizu, Y. Mikami, H. Mitani, K. Otsuka, *Trans. JIM*, **12**, 206 (1971).
18. C. Watanabe, T. Sakai, R. Monzen, *Philos. Mag*., **88**, 1401 (2008).
19. M. H. N Beshai, G. H. Deaf, G. Saad, S. B. Youssef, M. Sobhy, *Mater. Sci. Technol*., **27**, 184 (2011).
20. T. Hasegawa, Y. Takagawa, C. Watanabe, R. Monzen, *Mater. Trans*., **52**, 1658 (2011).
21. W. Bonfield, B. C. Edwards, *J. Mater. Sci*., **9**, 398 (1974).

22. M. A. Mahmoud, A. F. Abd El-Rehim, M. Sobhy, R.M. Abdel-Rahman, *Mater. Sci. Eng*. A **528**, 6026 (2011).
23. M. A. Mahmoud, G. Graiss, *J. Mater. Sci*., **37**, 2215 (2002).
24. M. H. N. Beshai, G. H. Deaf, A. M. Abd El-Khalek, G. Graiss, M. A. Kenawy, *phys. stat. sol*., (a) **161**, 65 (1997).
25. M. A. Mahmoud, A. F. Abd El-Rehim, *J. Mater. Sci*., **45**, 1579 (2010).
26. C. Watanabe, T. Sakai, R. Monzen, *Phil. Mag*., A **88**, 1401 (2008).
27. G. Graiss, M.A. Mahmoud, *J. Mater. Sci*. **36**, 1507 (2001).
28. T.S. Parel, S.C. Wang, M.J. Starink, *Mater. Des*. **31,** S2 (2010).
29. G. Dieter, Mechanical Metallurgy, *third ed., McGraw-Hill Co*., New York, (1986).
30. R.H. Nada, F. Abd El-Salam, L.A. Wahab, H.Y. Zahran, *Mater. Sci. Eng*. A **543**, 180 (2012).
31. H. Jiang, P. Bowen, J.F. Knott, *J. Mater. Sci*., **34**, 719 (1999).
32. G. Graiss, M.A. Mahmoud, *Fizika*, A **9**, 137 (2000).
33. R. H. Nada, F. Abd El-Salam, M. M. Mostafa, A. M. Abd El-Khalek, H. S. Mohammed, *J. Sci & Eng. Research*. **4**, 852 (2013).
34. [34] A. M. Abd El-Khalek, Effect of phase transformation and indium addition on workhardening characteristics of Al–Zn alloy, Mater. Sci. Technol. 28 (2012) 77.
35. F. Abd El-Salam, A. M. Abd El-Khalek, R.H. Nada, *Eur. Phys. J*., AP **12**, 159 (2000).
36. [36] M.A. Kenawy, G. Saad, G. Graiss, B. Beshai, *Sol. Stat. Comm*., **55**, 101 (1985).
37. G.S. Al-Ganainy, A. Fawzy, F. Abd El-Salam, *solid solution region*, *Physica*, B **344**, 443 (2004).